Geophys. J. Int. (2005) **160,** 1027–1043 doi: 10.1111/j.1365-246X.2005.02569.x

Spatiotemporal variations of crustal anisotropy from similar events in aftershocks of the 1999 *M*7.4 İzmit and *M*7.1 Düzce, Turkey, earthquake sequences

Zhigang Peng,*† and Yehuda Ben-Zion

Department of Earth Sciences, University of Southern California, Los Angeles, CA 90089-0740, USA

Accepted 2004 December 23. Received 2004 October 19; in original form 2004 August 2

SUMMARY

We analyse spatiotemporal variations of crustal anisotropy along the Karadere–Düzce branch of the North Anatolian Fault from similar earthquakes in the aftershock regions of the 1999 M_w7.4 İzmit and M_w7.1 Düzce earthquakes. The similar earthquake clusters are identified by performing cross-correlation on waveforms generated by ∼18 000 earthquakes. Depending on the applied similarity criterion, about 4–60 per cent of the events belong to similar event clusters. Splitting parameters averaged within each cluster show significant variations for slightly different ray paths, indicating strong spatial variations of crustal anisotropy in this area. We also find clear changes in the spatiotemporal seismicity patterns following the Düzce main shock. Large apparent co-seismic changes (up to 30 per cent) of shear wave splitting delay times are observed across the time of the Düzce main shock at stations near the epicentral region. However, the changes can be mostly explained by the spatial variations of ray paths due to the changing seismicity, rather than changes in the properties of the anisotropic medium. Splitting parameters measured within similar earthquake clusters indicate at most 2 per cent changes in delay times associated with the occurrence of the Düzce main shock. The results do not show systematic precursory changes before the Düzce main shock.

Key words: fault zone structure, seismic anisotropy, shear wave splitting, similar earthquakes.

1 INTRODUCTION

Large crustal fault zones are associated with belts of damaged rock characterized by high crack density and different seismic properties from those of the surrounding host rock (Ben-Zion & Sammis 2003, and references therein). The spatial extent and material properties of the damaged fault zone (FZ) rock have important implications for many aspects of earthquake behaviour (e.g. Lyakhovsky *et al.* 2001; Scholz 2002). One possible manifestation of damaged rock that has been used to infer FZ properties at depth is anisotropy due to preferential crack alignment parallel to the FZ structure (e.g. Leary *et al.* 1990, and references therein). In such a case, seismic shear waves propagating inside the FZ are expected to split into two orthogonally polarized waves with different velocities. This phenomenon is analogous to optical birefringence and is termed shear wave splitting. Two routinely determined splitting parameters are the polarization direction of the fast wave (ϕ) and the delay time (δt) between the fast and slow waves.

*Now at: Department of Earth & Space Sciences, University of California, Los Angeles, CA 90095-1567, USA.
†Corresponding author: Department of Earth & Space Sciences, University of California, Los Angeles, CA 90095-1567, USA. E-mail: zpeng@ess.ucla.edu.

Shear wave splitting has been claimed to provide an effective tool for detecting spatiotemporal variations of crustal anisotropy around active FZs, including monitoring the approaching times of major earthquakes (e.g. Crampin & Chastin 2003). However, these claims are controversial. A number of studies report temporal changes of splitting parameters before (e.g. Crampin *et al.* 1990, 1991, 1999; Gao *et al.* 1998), during (e.g. Saiga *et al.* 2003) and after (e.g. Tadokoro & Ando 2002) major earthquakes or swarms. However, other studies have observed no clear changes of crustal anisotropy near the epicentral regions of major earthquakes (e.g. Aster *et al.* 1990, 1991; Savage *et al.* 1990; Munson *et al.* 1995; Cochran *et al.* 2003; Liu *et al.* 2004, 2005).

Many of the previous studies on temporal changes of crustal anisotropy were based on analysis of waveforms with a mixture of ray paths sampling different regions of space. However, analysis results typically indicate large spatial variations in delay times (e.g. Vavryčuk 1993; Rabbel 1994) and fast directions (e.g. Zhang & Schwartz 1994; Tadokoro *et al.* 1999) within a given study area. Peng & Ben-Zion (2004) and Liu *et al.* (2004, 2005) have shown that spatial variations of anisotropy can be mapped erroneously into temporal changes. One effective way of separating spatial variations from temporal changes is to analyse shear wave splitting using clusters of similar earthquakes (e.g. Aster *et al.* 1990; Bokelmann & Harjes 2000). Such earthquakes are located

very close in space and they have nearly identical propagation paths to the recording stations (e.g. Poupinet *et al.* 1984; Nadeau *et al.* 1994). In addition, they have similar focal mechanisms and generate similar initial polarizations of shear waves. Since shear waves with different initial polarizations are sensitive to different sets of anisotropy (e.g. Peng & Ben-Zion 2004), it is important to use similar event clusters to remove spatial effects before searching for possible temporal changes of crustal anisotropy.

Peng & Ben-Zion (2004) performed a systematic analysis of shear wave splitting along the Karadere–Düzce branch of the North Anatolian Fault (NAF) and found approximately 1 km broad zones around the surface traces of the İzmit and Düzce main shocks with fault-parallel cracks or shear fabric. The belt of anisotropic rock surrounds an approximately 100 m wide seismic FZ waveguide generating trapped waves (Ben-Zion *et al.* 2003) and is confined primarily to the top 3–4 km of the upper crust. The results of Peng & Ben-Zion (2004) show large spatial variations of crustal anisotropy and suggest multiple mechanisms for the observed anisotropy in the area.

The present paper is a continuation of the work of Peng & Ben-Zion (2004) using similar earthquake clusters in the same data to perform a higher-resolution analysis of spatiotemporal variations of anisotropy. In the following sections, we first describe the methodology used to identify clusters of earthquakes with different degrees of similarity. We then combine the shear wave splitting measurements of Peng & Ben-Zion (2004) with the similar earthquake data obtained in this study and investigate the fine-scale spatial patterns and temporal changes of crustal anisotropy around the Karadere–Düzce branch of the NAF.

2 DATA

The analysis employs a large seismic waveform data set recorded by a temporary 10-station PASSCAL seismic network (Fig. 1) along and around the Karadere–Düzce branch of the NAF (Seeber *et al.* 2000; Ben-Zion *et al.* 2003). The seismometers were deployed a week after the 1999 August 17 M_w7.4 İzmit earthquake and operated for about 6 months. All 10 stations had REFTEK recorders and three-component L22 short-period sensors with a sampling frequency of 100 Hz. The temporary seismic network straddled the rupture zones of both the İzmit and the 1999 November 12 M_w7.1 Düzce main shocks and recorded about 26 000 earthquakes during its operational period. The event locations were obtained with standard HYPOINVERSE determinations (Klein 1978) and station corrections. The horizontal location errors are less than 1 km around the centre of the network and 1–2 km near the margins. The vertical errors are somewhat greater. In this study we focus on ∼18 000 earthquakes that are located within ∼20 km of the network and are recorded by at least three of the 10 stations. Additional details on the seismic experiment and data set are given by Seeber *et al.* (2000) and Ben-Zion *et al.* (2003).

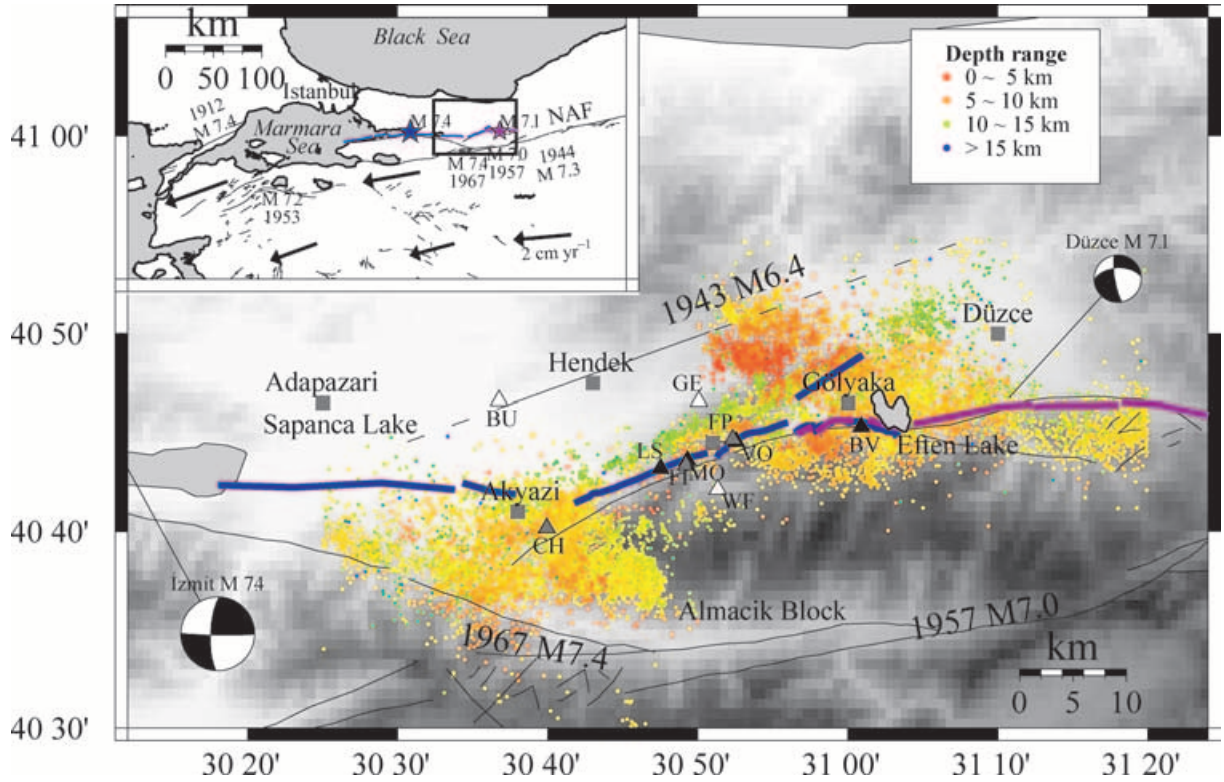

Figure 1. Hypocentral distribution of ∼18 000 earthquakes recorded by the PASSCAL seismic experiment along the Karadere–Düzce branch of the NAF. Aftershock locations are marked by small dots with colours denoting different depth ranges. The shaded background indicates topography with white being low and dark being high. The surface ruptures of the İzmit and Düzce earthquakes are indicated with thick blue and purple lines, respectively. Dark thin lines associated with earthquake information denote faults that were active during recent ruptures. Other dark thin lines are geologically inferred fault traces. Stations within, near and outside the FZ are shaded with dark, grey and white triangles, respectively. Grey squares denote locations of nearby cities. The inset illustrates the tectonic environment in northwestern Turkey with the box corresponding to our study area. Arrow vectors represent the plate deformation rate (Reilinger *et al.* 1997) from GPS data. Modified from Peng & Ben-Zion (2004).

3 ANALYSIS PROCEDURE

To reduce the mixing of spatial and temporal effects in the data, we use clusters of similar earthquakes identified by performing cross-correlation calculations (Aster & Scott 1993). To reduce the calculation load, we restrict the waveform cross-correlation for event pairs with hypocentral separations $\leq$10 km. This value is several times larger than the location errors of the events. The cross-correlation is computed over a time window spanning 0.5 s before and 1.5 s after the *P*-wave arrival for the vertical-component seismogram, and 1 s before and 2 s after the *S*-wave arrival for the horizontal-component seismograms. Fig. 2 shows examples of north-component waveforms at station FP having different values of correlation coefficients (CC) with respect to the first waveform. Generally, waveforms with high CC values have similar shapes and are likely to be generated by earthquakes that have similar locations and focal mechanisms.

Fig. 3 gives the distribution of the CC values and correlation lag times for all north-component waveform pairs recorded at station FP. Most CC values are distributed between 0.2 and 0.5, indicating that the corresponding waveform pairs are poorly correlated. However, a small percentage of CCs are distributed above 0.7, suggesting the existence of groups of events that generate similar waveforms. The wide spread of the lag times at high CCs indicates that the automatically picked *P*- and *S*-wave arrivals that are used for initial alignment of the waveform pairs are not self-consistent and accurate.

Next, we define a similarity measure (β) between two events using the median value of the *P* and *S* correlation coefficients at all the stations that recorded the examined pair of events. The median is chosen instead of the mean value since the mean is sensitive to outliers with very low CCs (Aster & Scott 1993). Fig. 4 shows values of the median CCs versus hypocentral separations between pairs of events for the $\sim$18 000 earthquakes employed. Most median CC values are distributed between 0.2 and 0.5 even for event pairs with small hypocentral separations (e.g. $<$2 km), indicating that events with similar locations can generate quite different waveforms, possibly due to different focal mechanisms. On the other hand, the existence of high median CC values (e.g. $>$0.9) with large (e.g. $>$5 km) hypocentral separations suggests that the original hypocentral locations based on the HYPOINVERSE algorithm and station corrections may contain errors.

Finally we organize the earthquakes into clusters of similar events using an equivalency class (EC) algorithm (e.g. Press *et al.* 1986). The EC algorithm identifies pairs of events that satisfy a given similarity criterion ($\beta \geq \beta_c$) and groups such pairs that share an event into similar earthquake clusters. For example, if event pairs (A, B) and (B, C) both satisfy the criterion, A, B and C will be grouped into one cluster, regardless of the similarity measure between A and C. In practice, we include an event pair in a cluster only if the waveforms of the pair were recorded by three or more stations.

The number and size of the obtained similar earthquake clusters vary depending on the similarity criterion β_c. Fig. 5 illustrates that dependency for the $\sim$18 000 earthquakes. If the β_c value is close to 1, the EC algorithm produces a small number of clusters with a small number of events in each cluster having highly similar waveforms. As the β_c value is somewhat reduced, new events are included, resulting in an increase in the number of clusters and the number

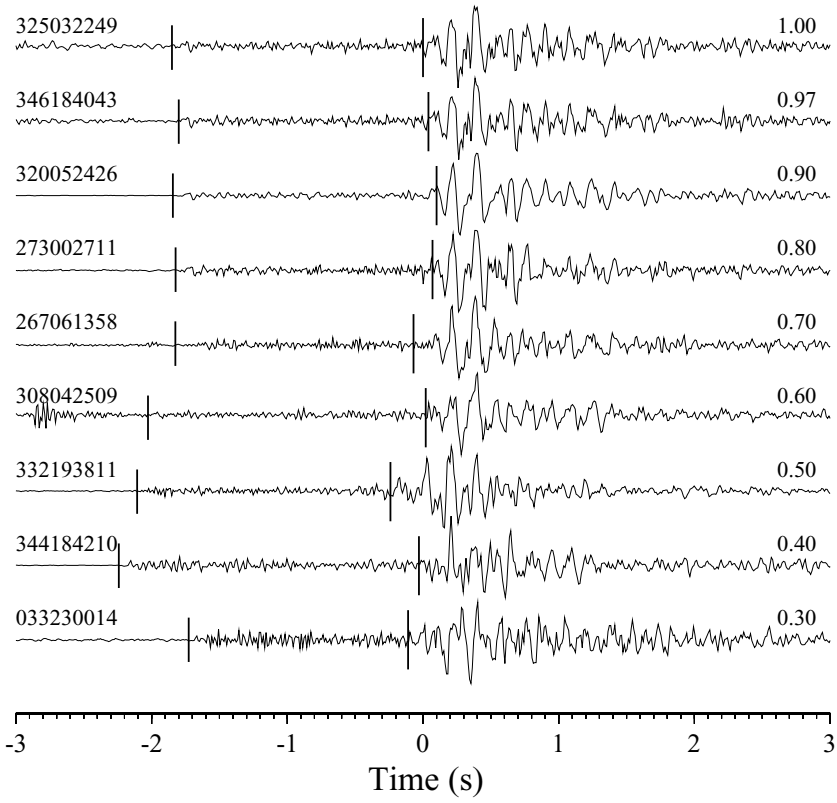

Figure 2. Examples of waveform similarity for north-component seismograms recorded at station FP. The short solid vertical bars denote the routinely picked *P* and *S* arrivals. The waveform generated by each event is cross-correlated with that of event 325032249 over a time window of 1 s before and 2 s after the *S* arrivals. The corresponding correlation coefficient is marked on the right of each trace. The event ID number consists of three-digit Julian day, two-digit hour, two-digit minute and two-digits seconds of the earthquake occurrence time. Julian days in the range 237–365 are in the year 1999 and those in the range 001–042 are in 2000.

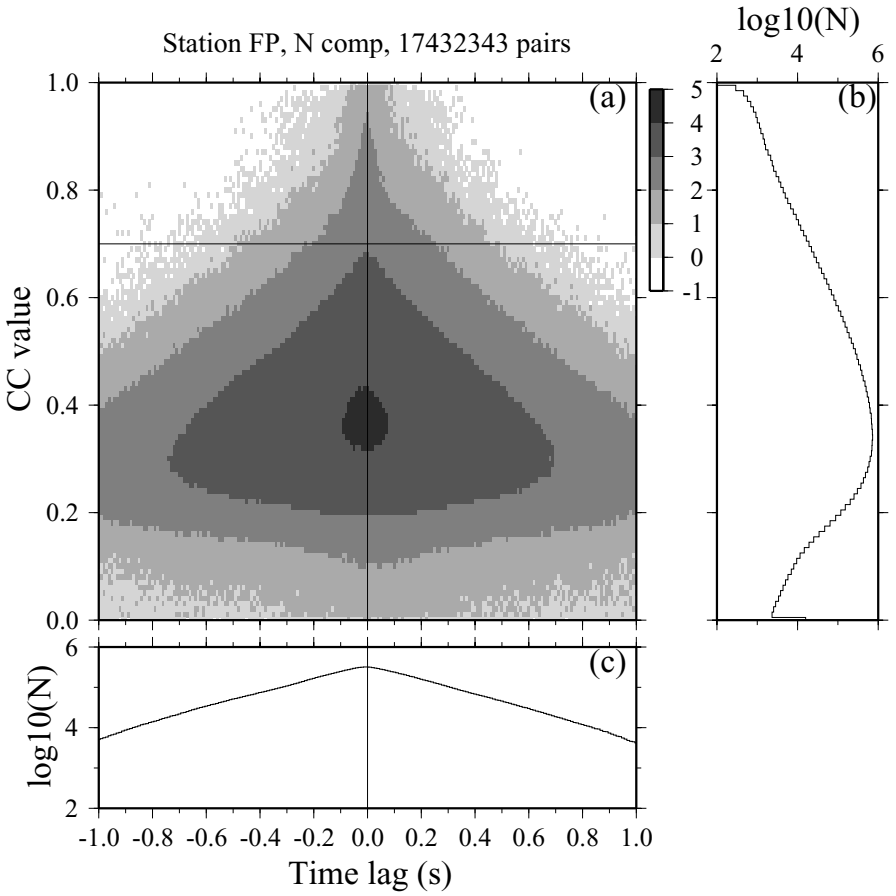

Figure 3. (a) The correlation coefficients (CC) for $\sim 17 \times 10^6$ north-component waveform pairs recorded at station FP versus their time lags. Contours show the logarithmic number of event pairs over a grid cell of size 0.01 × 0.01 s for CC and time lags. The vertical and horizontal lines mark the zero lag time and CC value of 0.7, respectively. About 0.8 per cent of all the waveform pairs have CC values higher than 0.7. (b) Histogram of the CC. (c) Histogram of the time lags.

of events in each cluster. However, reducing the β_c value below some level (e.g. <0.7) leads to the merging of two or more formerly separate clusters and a decease in the total number of clusters.

For β_c values between 0.95 and 0.70, approximately 4–60 per cent of the events in our data set belong to similar event clusters (Table 1). The resulting percentage range is slightly higher than those from the aftershock sequence of the 1994 Northridge, California, earthquake (Shearer *et al.* 2003) and microearthquakes recorded by the Anza seismic network (Aster & Scott 1993), but lower than the values from recent studies of seismicity at the Parkfield and other active strands of the San Andreas and other faults in central and northern California (e.g. Nadeau *et al.* 1995; Rubin *et al.* 1999; Schaff *et al.* 2002). Such a comparison is qualitative, however, since the methods employed to identify similar event clusters in these studies are not exactly the same.

4 RESULTS

4.1 Spatiotemporal evolutions of similar event clusters and seismicity

Figs 6 and 7 show locations of similar event clusters with similarity criteria $\beta_c = 0.95$ and 0.70, respectively. The events with $\beta_c = 0.95$ are likely to rupture the same patch of the fault repeatedly and are termed repeating earthquakes (e.g. Nadeau *et al.* 1995; Igarashi *et al.* 2003). Lower β_c values (e.g. 0.70) represent events that are located close to each other and have similar focal mechanisms, but may not rupture the same patch (e.g. Lees 1998; Shearer *et al.* 2003). Since the obtained temporal variations of splitting parameters are very sensitive to changes of earthquake locations, we use clusters with $\beta_c = 0.70$ only to investigate the fine-scale spatial patterns of crustal anisotropy. This similarity criterion is chosen because the number of similar event clusters with at least five events (nclust5) reaches its maximum at $\beta_c = 0.7$ (Fig. 5). A high-resolution analysis of temporal changes of crustal anisotropy is done using the tighter repeating earthquake clusters identified with $\beta_c = 0.95$. Such a cut-off value represents a compromise between the need for highly repeatable sources and the need to have a reasonable number (nclust5 = 40) of clusters for the analysis. It is interesting to note that the similar event clusters with $\beta_c = 0.95$ around the Düzce segment (cross-section BB′) are distributed throughout the seismogenic zone, while clusters with $\beta_c = 0.95$ along the ∼30 km Karadere segment (cross-sections AA′ and CC′) are confined primarily to the 12–15 km depth range near the bottom of the seismogenic zone.

The seismicity in our data set exhibits complex spatiotemporal evolution that can affect our inferences on changes of anisotropy and other material properties. The occurrence of the Düzce main shock produces changes of stress that are expected to increase the seismicity rate in some places and decrease it in others. Fig. 8 compares the seismicity rates in our data set before and after the Düzce main shock. The change in seismicity rate at time t over each grid cell of size 1.2 km × 1.2 km is represented by a statistical Z value

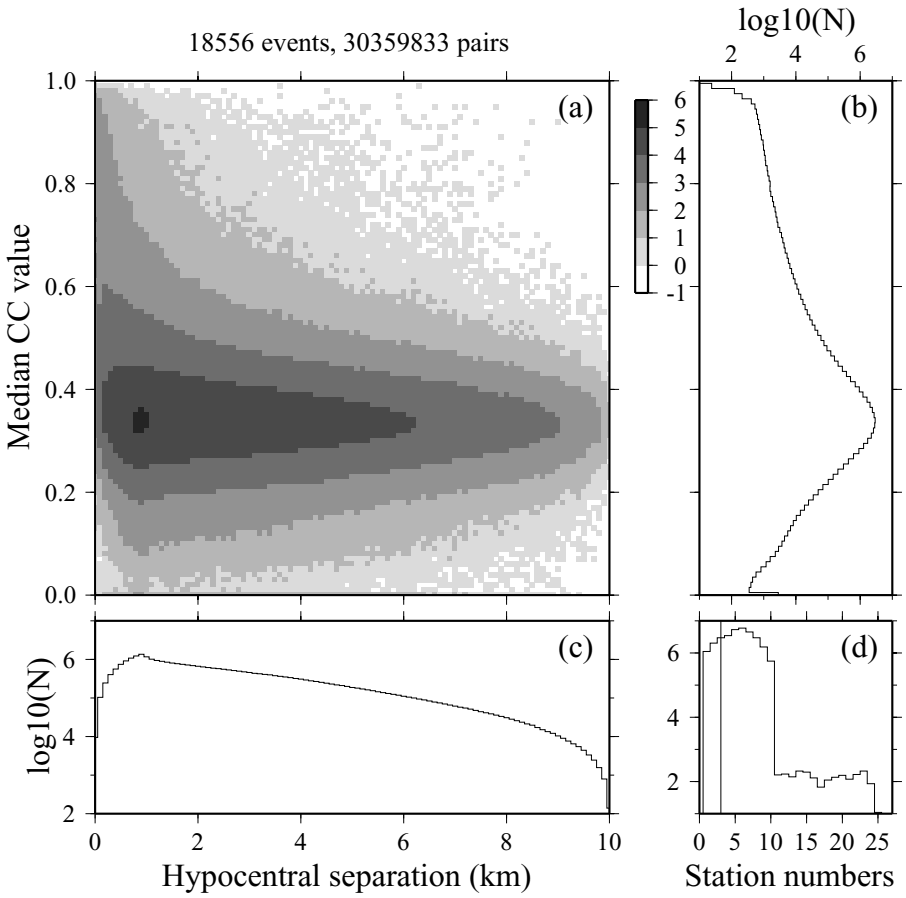

Figure 4. (a) The median CC values (similarity measure β) for $\sim 30 \times 10^6$ pairs of waveforms recorded at station FP versus their hypocentral separation D. Contours show the logarithmic number of waveform pairs over grid cell of size 0.1 km $\times$ 0.01 for D and β. (b) Histogram of the similarity measure β. (c) Histogram of the hypocentral separation D. (d) Histogram of the number of recording stations that pairs of events have in common. The vertical line marks the cut-off value of at least three stations that are used in the similar earthquake identification analysis.

Table 1. Number of clusters and similar earthquakes (total events: 18 556).

β_c	nclust	nclust5	nev	nev5	Percentage
0.95	257	40	803	326	4.3
0.90	1068	109	3242	1011	17.5
0.85	1712	259	5834	2406	31.4
0.80	2093	349	8023	3824	43.2
0.75	2125	415	9387	5618	52.7
0.70	2000	442	11366	7566	61.3

β_c is the similarity criterion, nclust is the total number of similar event clusters, nclust5 is the number of similar event clusters with at least five events, nev is the number of events belonging to similar event clusters, nev5 is the total number of events that are similar to at least five or more events, and the percentage is nev divided by the total events number.

(Habermann 1983; Wiemer 2001), with positive and negative numbers indicating decrease and increase in rate, respectively. It is seen that the seismicity rate increases around the east portion of the Düzce rupture zone and to the north of the west part of the main shock, while it decreases south of that part and further to the west.

In Section 4.3, we present delay times between fast and slow shear waves derived from seismic records at various stations over about a 6-month period spanning the time of the Düzce main shock. It is clear from Fig. 8 that such data are associated with sources subjected to considerable spatiotemporal fluctuations and cannot be lumped in a careful study of temporal changes of anisotropy properties. We therefore analyse in Section 4.4 temporal changes of anisotropy properties using repeating event clusters that sample closely similar propagation paths at different times.

4.2 Fine-scale spatial variations of anisotropy

Due to uncertainties in the shear wave splitting measurements, previous studies of crustal anisotropy often average splitting parameters based on source–receiver locations or spatial regions (e.g. Cochran *et al.* 2003; Peng & Ben-Zion 2004). However, as shown in Fig. 4, earthquakes from similar regions can generate dissimilar waveforms with different initial polarizations of shear waves (e.g. due to different focal mechanisms). Peng & Ben-Zion (2004) pointed out that shear waves with different initial polarizations may sample different sets of microcracks in a complex region, resulting in a scattered or bimodal distribution of splitting measurements. Thus averaging splitting measurements based solely on spatial regions may reduce the resolution of the obtained results.

A better way to group and present the splitting measurements is to average within each cluster splitting parameters that have similar waveforms, similar propagation paths and similar initial shear wave polarizations. To obtain a high-resolution spatial distribution of crustal anisotropy in our study area, we average the high-quality splitting parameters of Peng & Ben-Zion (2004) within each similar earthquake cluster having a similarity criterion $\beta_c = 0.70$. We use

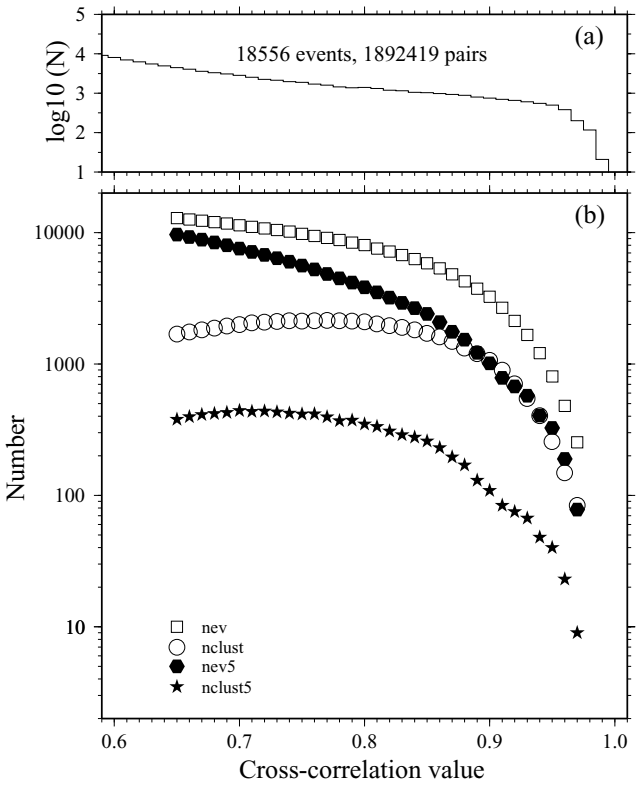

Figure 5. (a) Histogram of the similarity measure β between pair of events that are recorded by at least three stations between pairs of events and $\beta \geq 0.65$. (b) Number of events that belong to a cluster (nev), number of events belonging to a cluster with five or more events (nev5), total number of similar event clusters (nclust), and number of clusters with at least five events (nclust5) as a function of the similarity criterion β_c.

the von Mises method to calculate the mean angle of the fast direction and a mean resultant length R (Davis 1986; Mardia & Jupp 2000; Cochran *et al.* 2003). The parameter R gives a quantitative estimate of the variance of the directional data, with values near 0 and 1 indicating high scattering and clustering, respectively. In addition, we compute the standard error of the mean fast direction using the formula $1/\sqrt{(\kappa n R)}$, where κ is the maximum likelihood estimate of the concentration parameter and n is the number of samples (Davis 1986).

We select clusters that have four or more high-quality splitting measurements with standard error of the mean fast direction less than 10°. We then present the average splitting parameters in the following two ways. First, the average splitting parameters for 9 of the employed 10 stations are plotted on top of the centroid location of each cluster (Fig. 9). The results for station BU are not shown because we have only two clusters with more than four high-quality measurements at this station. For stations CH, FI, VO, FP and BV that are inside or within ∼1 km of the surface ruptures of the İzmit and Düzce main shocks, the dominant fast directions (ϕ values) are parallel or subparallel to the direction of the nearby fault strike. However, stations that are within the İzmit rupture zone (e.g. LS, MO and VO) generally have more scattered fast directions. The results show clearly that similar earthquake clusters with different ray paths produce quite different ϕ values. This observation indicates strong spatial variations of crustal anisotropy in this area.

Second, the average splitting parameters for nine clusters that have splitting parameters at four or more stations are plotted together on top of the recording station (Fig. 10). The average splitting parameters for the same group of earthquakes within each cluster are different at stations separated by a few kilometres, indicating that the observed anisotropy does not originate near the source. In addition, we observe quite different splitting parameters for several clusters at FZ station pairs MO–FI (e.g. C02: ϕ[MO] = 150 ± 9°, δt[MO] = 0.09 ± 0.04 s; ϕ[FI] = 86 ± 7°, δt[FI] = 0.06 ± 0.01 s) and VO–FP (e.g. C15: ϕ[VO] = 99 ± 5°, δt[VO] = 0.06 ± 0.04 s; ϕ[FP] = 43 ± 6°, δt[FP] = 0.08 ± 0.05 s) that are located only several hundred metres apart. Peng & Ben-Zion (2004) found no clear dependency of splitting delay time δt with increasing depth or hypocentral distance for most stations, and concluded that the anisotropy is confined primarily to the top 3–4 km of the crust around the Karadere–Düzce faults. The observation of variable splitting parameters over short distances (e.g. several hundreds of metres) indicates that near-station fault structures play an important role in producing the shear wave splitting and further support the shallow anisotropy interpretation in our study area. For propagation paths inside the Almacik Block south of the Karadere segment (e.g. C01), stations LS, MO, FI and WF record similar splitting parameters, indicating a relatively uniform anisotropy within the block that is possibly caused by lithological properties (Peng & Ben-Zion 2004).

In summary, splitting parameters for earthquakes within the same cluster are generally very similar at a given station (e.g. about 70 per cent of the clusters have R value ≥0.8 and the standard deviation of the average delay times of ≤0.03 s). However, different splitting parameters are observed for earthquake clusters that are located nearby, and for stations that are separated by several hundred metres. The overall spatial variations based on similar earthquakes are consistent with the results of Peng & Ben-Zion (2004) and confirm that multiple structures and mechanisms contribute to the observed crustal anisotropy in the area. The observation of large spatial variations of crustal anisotropy plays an important role in explaining the apparent temporal changes of splitting parameters in the following section.

4.3 Apparent temporal variation of anisotropy

Since our temporary seismic network straddles the rupture zones of both the İzmit and Düzce main shocks, many tens of thousands of waveforms were recorded during its 6-month operational period (Seeber *et al.* 2000; Ben-Zion *et al.* 2003). This allows us to evaluate carefully the hypothesis that temporal changes of anisotropy are correlated with the time of a major earthquake (e.g. Crampin *et al.* 1999). We first check the splitting results at station BV, which is very close to the hypocentral region of the Düzce main shock and inside its surface rupture zone. Fig. 11 compares the hypocentral locations and the high-quality splitting parameters of ∼700 earthquakes before and after the Düzce earthquake. There appears to be a 22 ms (∼30 per cent) increase in the average delay time δt and a ∼7° rotation of the average fast direction ϕ at the time of the Düzce main shock. However, as shown in Fig. 11(a), the source locations have also changed considerably. A shift of ∼7 km in the average hypocentral locations is observed before and after the Düzce main shock. Peng & Ben-Zion (2004) found that the average δt for station BV from ray paths along the ∼65° north-dipping main shock rupture zone (Utkucu *et al.* 2003) are much larger than those from the south side of the fault. Thus, the observed apparent 30 per cent co-seismic change of splitting parameters is most probably caused by spatial variations associated with changes of event locations, rather than by temporal changes of the anisotropic medium.

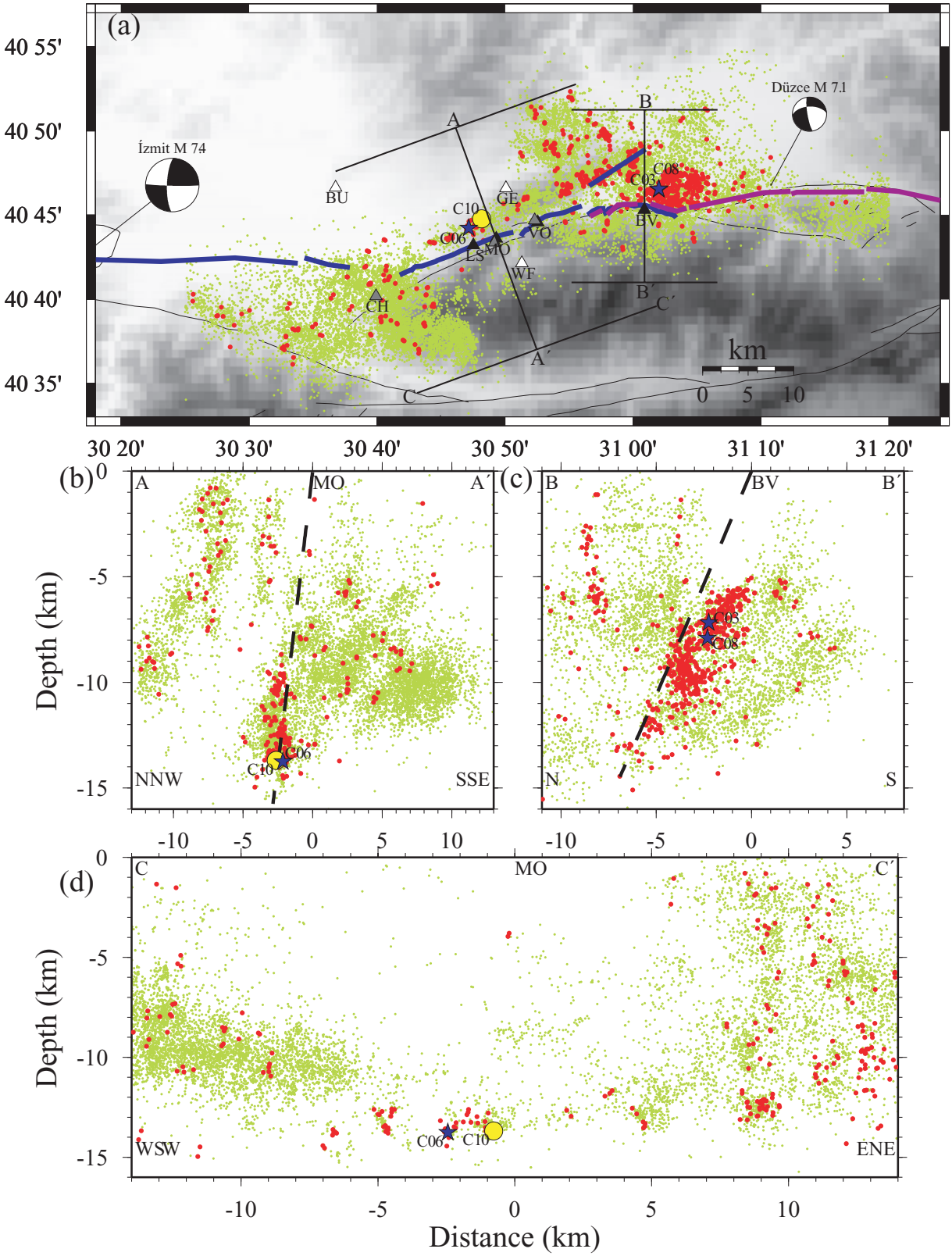

Figure 6. A map view (a) and three cross-sections (b–d) showing repeating earthquake clusters (red) with similarity criterion $\beta_c = 0.95$ with respect to the overall seismicity (light green) along the Karadere–Düzce branch of the NAF. The surface ruptures of the İzmit and Düzce earthquakes are indicated with thick blue and purple lines, respectively. The dashed lines in (b) and (c) indicate the ∼80° north-dipping fault along the Karadere segment that ruptured during the İzmit earthquake and the ∼65° north-dipping fault that ruptured during the Düzce earthquake, respectively. The average hypocentral location for cluster C10 is denoted with the yellow circle. Splitting parameters for earthquakes belonging to this cluster are shown in Figs 13–15. The blue stars mark the average locations for clusters C03, C06 and C08 that are used in Fig. 15. Other symbols and notations are the same as in Fig. 1.

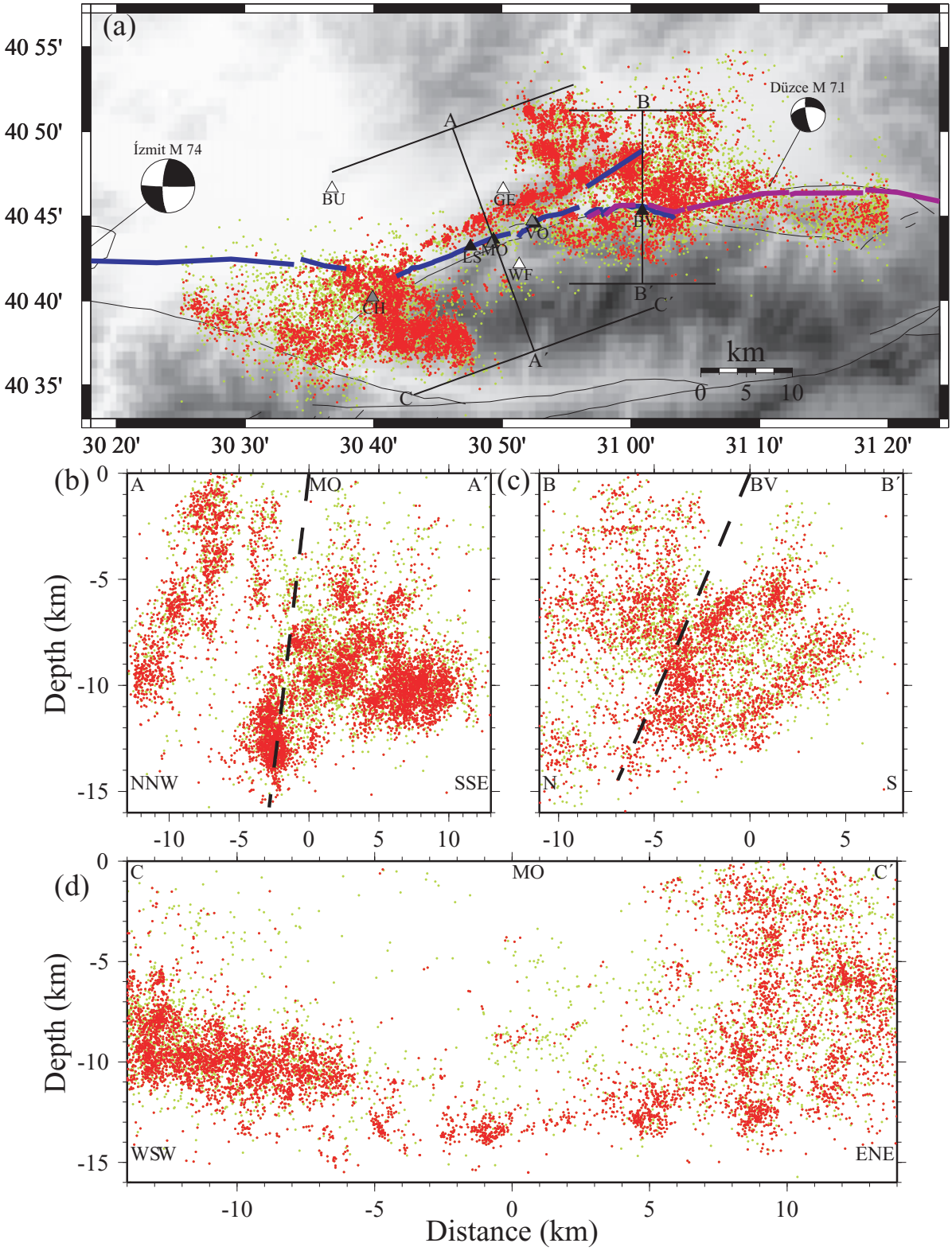

Figure 7. A map view (a) and three cross-sections (b–d) showing similar earthquake clusters (red) with similarity criterion $\beta_c = 0.70$ with respect to the overall seismicity (light green) along the Karadere–Düzce branch of the NAF. Other symbols and notations are the same as in Fig. 6.

Studies attempting to detect temporal changes of anisotropy typically use five-point running average of the data (e.g. Crampin *et al.* 1999; Saiga *et al.* 2003). Such a line in Fig. 11(b) suggests a slight increase of delay time δt about 2 weeks before the main shock. However, similar fluctuations are observed at other periods, and the more refined analysis in Section 4.4 with repeating events does not show a similar temporal change.

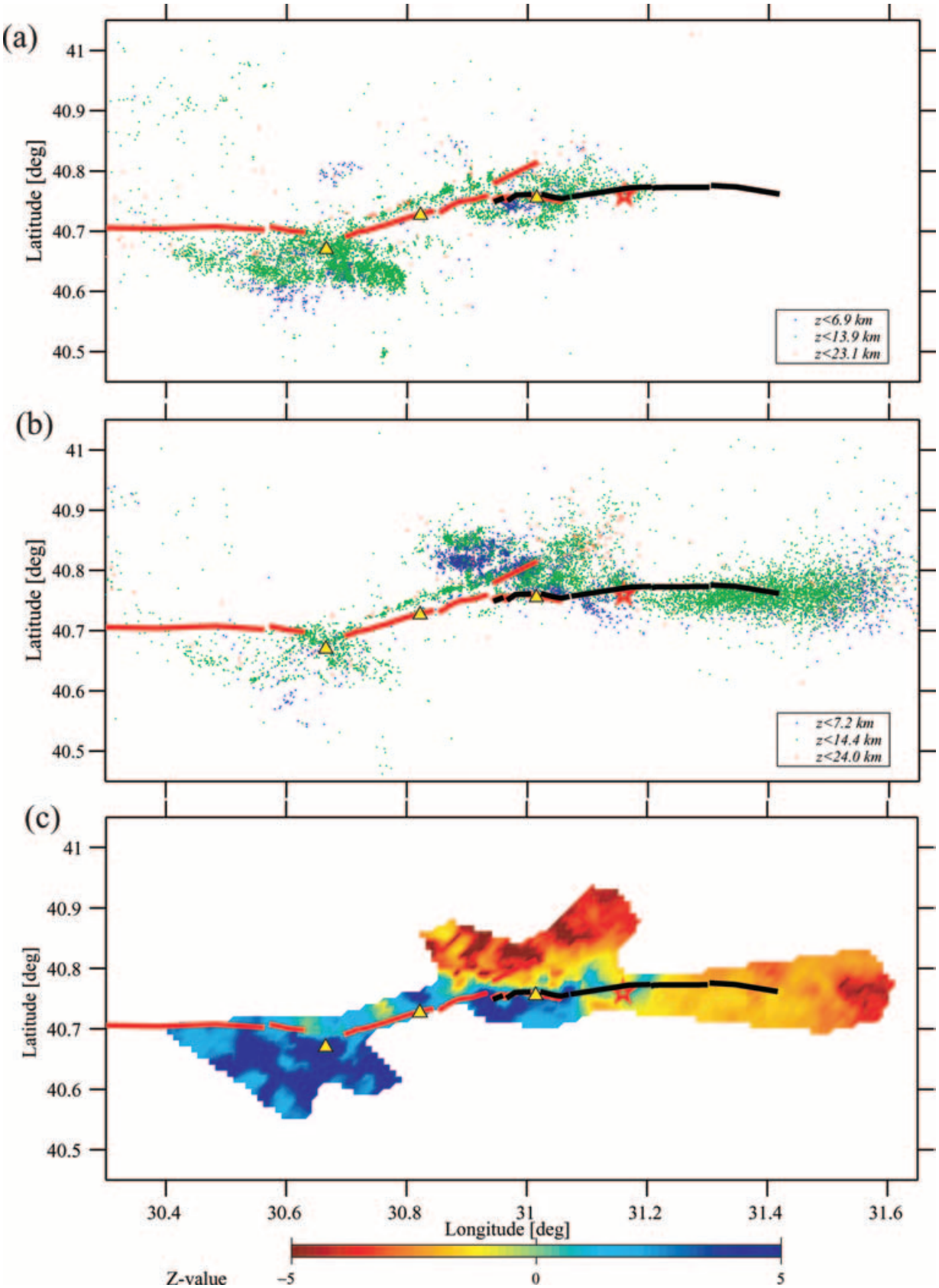

Figure 8. Locations of earthquakes that occurred before (a) and after (b) the Düzce main shock (red star). Earthquake locations are marked by small dots with colours denoting different depth ranges. The surface ruptures of the İzmit and Düzce earthquakes are indicated with red and dark lines, respectively. The three yellow triangles from left to right denote the locations of stations CH, MO and BV, respectively. (c) *Z*-value map of the seismicity rate change before and after the Düzce main shock. Positive *Z*-values (blue) represent a rate decrease, while negative values (red) represent an increase.

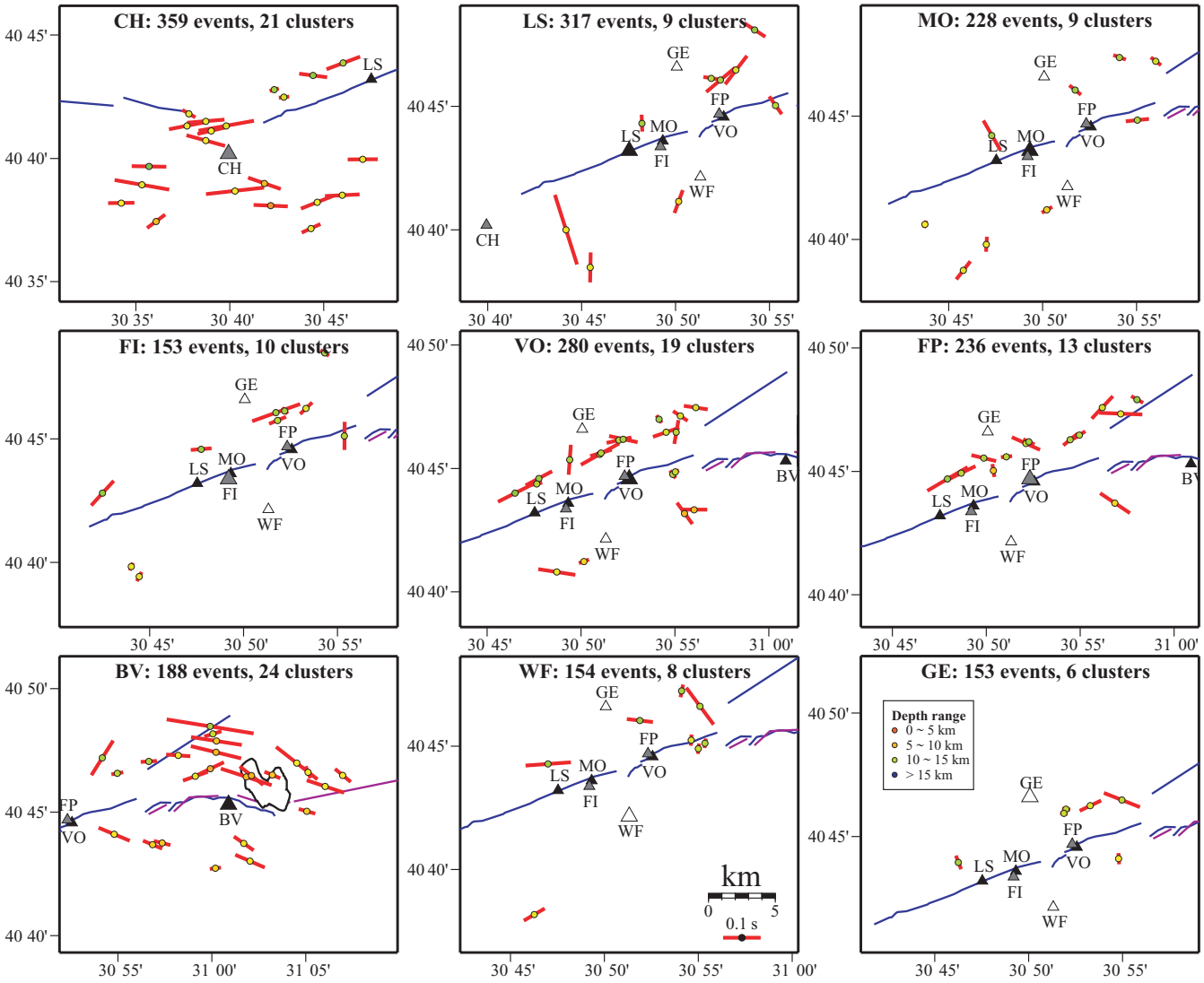

Figure 9. Average splitting parameters (red bars) for different similar event clusters with similarity criterion $\beta_c = 0.70$ at nine stations. Splitting parameters are averaged within each cluster having at least four individual measurements and standard error of the mean fast direction no more than 10°. The bar is oriented parallel to the average fast direction ϕ and scaled by the average delay time δt. The centre of each bar (circle) is plotted on top of the average source epicentre with colours denoting different depth ranges. Stations within, near and outside the FZ are shaded with dark, grey and white triangles, respectively. The total numbers of the earthquakes and clusters for each station are marked on top of each panel. The surface ruptures of the İzmit and Düzce earthquakes are indicated with blue and purple lines, respectively.

Fig. 12 gives the temporal changes of delay times at eight other stations. Results for station GE are not shown since most of the east component waveforms before the Düzce main shock were not recorded properly. Changes of average delay times ranging from 1–10 per cent are observed before and after the Düzce main shock for these eight stations. However, the delay time measurements are scattered over large ranges (up to 0.3 s). As shown in the next section, co-seismic changes of splitting delay times within repeating event clusters are less than 2 per cent. Thus, the apparent co-seismic changes in Figs 11 and 12 are probably dominated by spatial variations of seismicity and corresponding changes of ray paths.

4.4 Fine-scale temporal variations of anisotropy

The results of Section 4.1 show that the occurrence of the Düzce earthquake significantly changes the spatiotemporal seismicity patterns along the Karadere–Düzce branch of the NAF. We also observe from the average splitting parameters within similar event clusters large spatial variations of crustal anisotropy in this area (Section 4.2). In Section 4.3, we show that the large spatial variations of anisotropy can be mapped into temporal variations by the changing seismicity. To examine more closely temporal variations of anisotropic properties, we now analyse splitting parameters generated by repeating event clusters with a high similarity criterion ($\beta_c = 0.95$).

In general, there are two ways to estimate temporal variations of shear wave splitting delay times. The most common way is to first calculate the delay time δt between the fast and slow waves for each event and then compare the obtained delay times with a reference measurement. Fig. 13 shows splitting parameters measured from 10 earthquakes that belong to the repeating earthquake cluster C10. To obtain a subsample accuracy, we interpolate the waveforms from 100 samples to 10 000 samples per second using the SAC routine 'interpolate' (e.g. Niu *et al.* 2003). The *S*-wave arrivals are realigned by matching the waveform to that of the first event. Fig. 13(b) shows

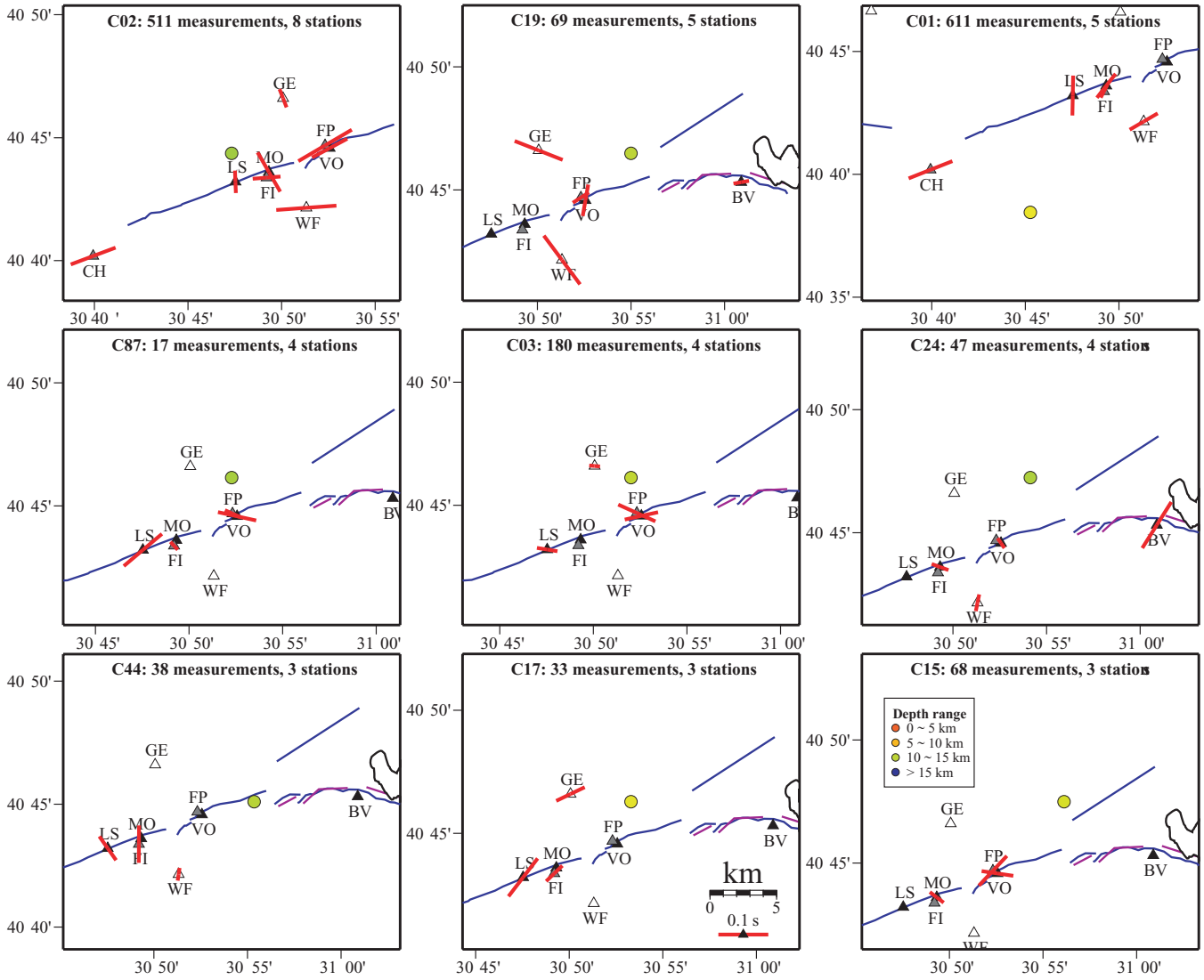

Figure 10. Average splitting parameters (red bars) at different stations for nine clusters with similarity criterion $\beta_c = 0.70$. The centre of each bar is plotted on top of the recorded station. The circle in each panel denotes the average epicentre of that cluster with colour denoting different depth ranges. The total numbers of measurements and recording stations are marked on top of each panel. Other symbols and notations are the same as in Fig. 9.

an increase of ~2.4 ms for the average delay times δt before and after the Düzce main shock, corresponding to a ~1.3 per cent anisotropy change with an average δt value of 0.182 s. However, the differences of *S*–*P* times exhibit a similar pattern (Fig. 13a), suggesting that the subtle change of the δt values could still be caused by spatial variations of the event locations.

Another way to measure temporal changes of delay times is to start by calculating the relative time differences of the fast and slow waves separately as $\Delta(\delta t) = \Delta(t_s - t_f) = (t_s - t_f) - (t_s - t_f)^{REF} = (t_s - t_s^{REF}) - (t_f - t_f^{REF}) = \Delta(t_s) - \Delta(t_f)$, where t_f and t_s represent the traveltime of the fast and slow waves, respectively (Bokelmann & Harjes 2000). Fig. 14 illustrates how we measure the relative time difference of the fast and slow waves recorded at station FP for the 10 events in cluster C10. We first rotate the two horizontal seismograms into fast and slow components using the average fast direction obtained in Fig. 13(c). The use of the average direction is justified by the fact that the observed fast direction remains nearly constant for most similar event clusters (e.g. Fig. 13c). Since both the origin time of an event and the absolute timing of a seismogram may contain errors that are larger than several milliseconds, seismograms are aligned by matching waveforms of the *P* phases to that of the first event. The relative time difference for each set of fast and slow shear waves from those of the first event are then calculated by waveform cross-correlation. The obtained high cross-correlation coefficients ($\geq$0.98) indicate that the waveform shapes of the fast and slow waves for these events are nearly identical. In addition, the relative traveltime changes of the fast $\Delta(t_f)$ and slow $\Delta(t_s)$ waves (Figs 14c and d) are of the order of milliseconds and are nearly synchronized. After subtracting $\Delta(t_s) - \Delta(t_f)$, the resulting relative delay times between the fast and slow waves are less than 1 ms, corresponding to a 0.4 per cent change of anisotropy at station FP along the propagation path associated with the employed cluster.

Fig. 15 summarizes results from such analysis for four clusters at five stations that contain at least five high-quality splitting measurements. The changing trends of the fast (Fig. 15a) and slow (Fig. 15b) waves are very similar, resulting in very small variations in the relative delay times (Fig. 15c). As seen in Fig. 15(d), the results put an upper bound of a 2 per cent change of delay

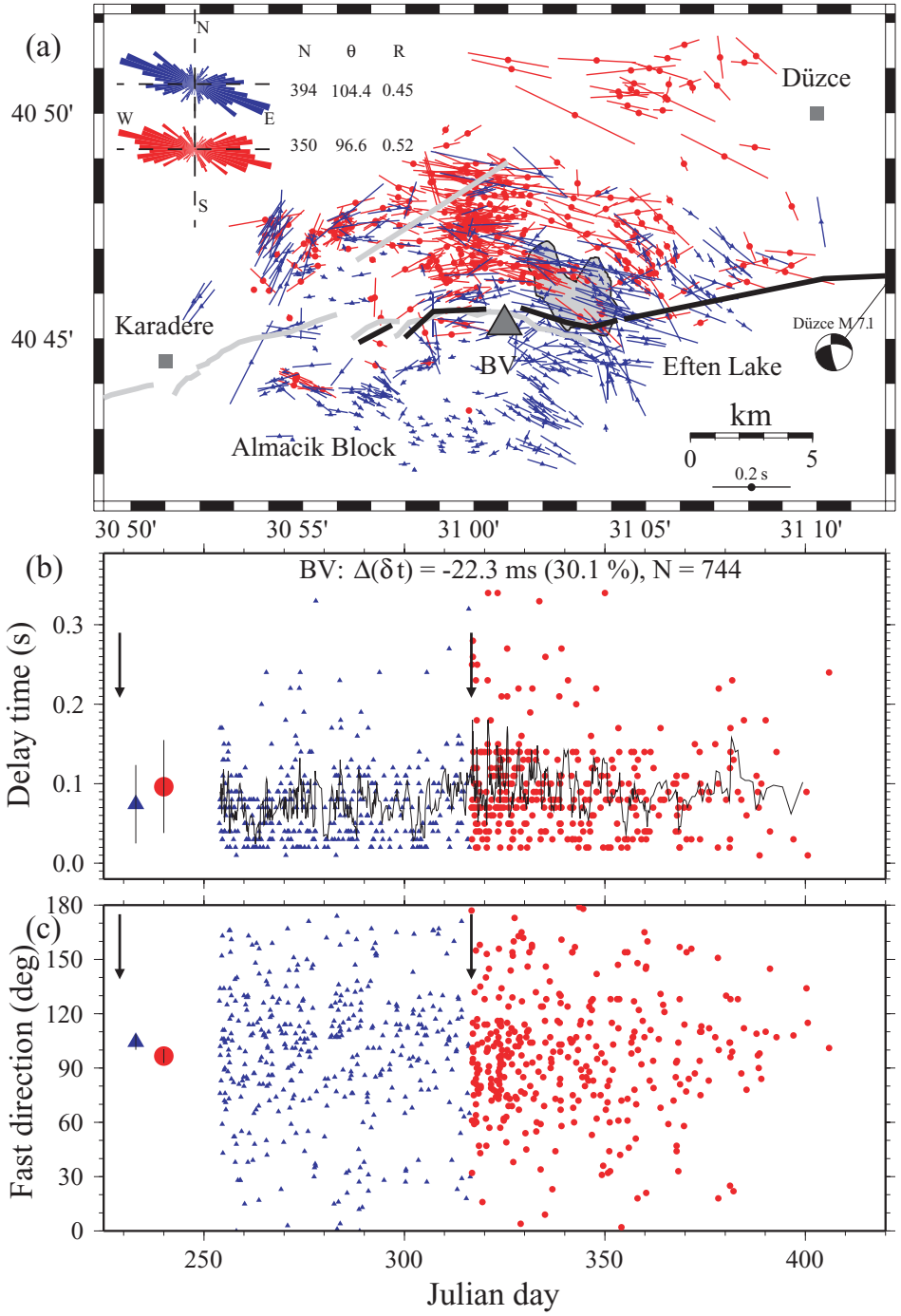

Figure 11. (a) Splitting parameters (bars) for station BV superimposed on the hypocentral locations of ~700 earthquakes. The bar is oriented parallel to the fast polarization direction ϕ and scaled by the delay time δt. Blue and red colours denote results for earthquakes before and after the Düzce earthquake, respectively. The rose diagrams of the fast directions, total number of measurements (N), average fast direction (θ) and the mean resultant length (R) are marked at the top left corner. (b) Delay times measured at station BV plotted against the earthquake occurrence times (Julian day since 1999). The two arrows mark the time of the İzmit and Düzce earthquakes. Small blue triangles and red circles denote measurements before and after the Düzce earthquake. The bigger blue triangle and red circle with vertical lines give the mean and standard deviations of all the measurement before and after the Düzce earthquake, respectively. The thin dark line is a five-point running average of the delay time measurements. The station name, change of the average delay time $\Delta(\delta t)$ with the corresponding percentage, and the total number of measurements are marked on the top. (c) Fast directions plotted against earthquake occurrence times. Other symbols and notations are the same as in (b).

time of fast and slow shear waves during the 6-month period of the study. These high-resolution observations do not show systematic changes of relative delay times before the Düzce main shock.

5 DISCUSSION

We perform a systematic high-resolution analysis of spatiotemporal variations of crustal anisotropy along and around the

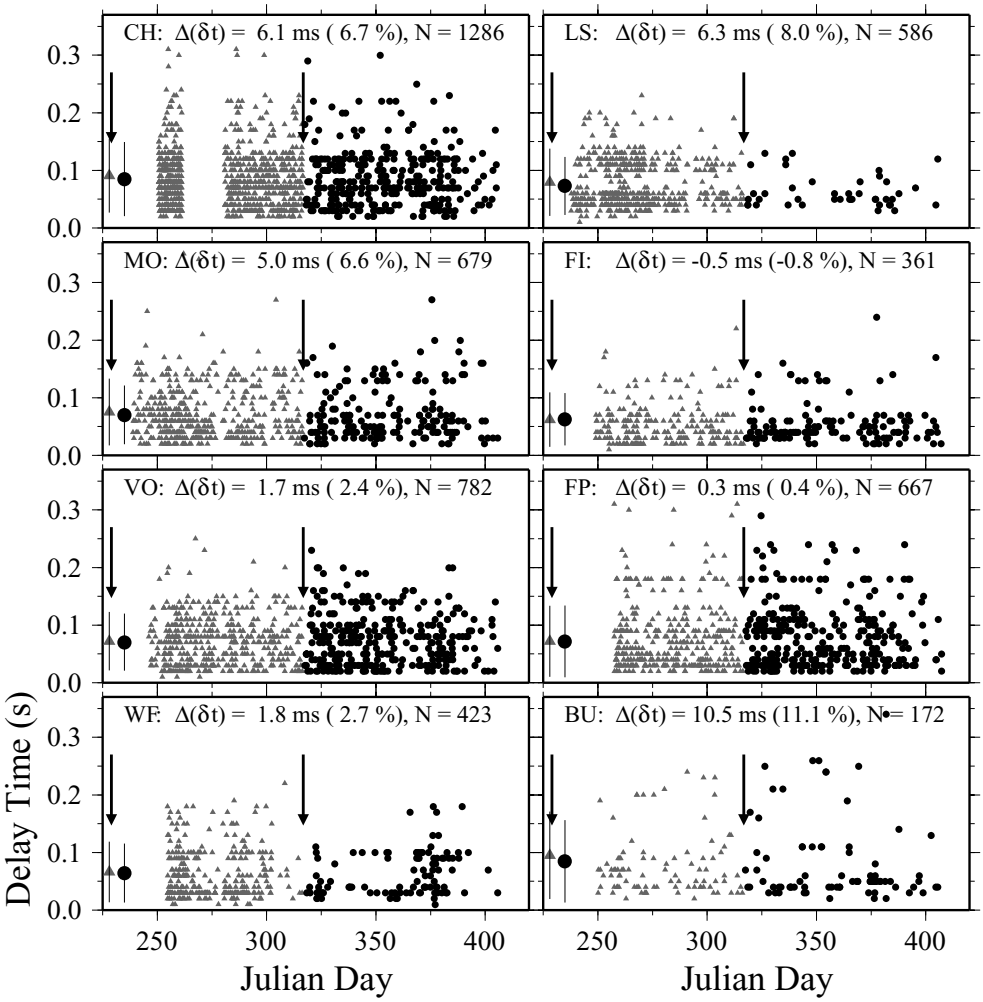

Figure 12. Delay times plotted against the earthquake occurrence times for eight stations. Grey and dark shades denote results for earthquakes before and after the Düzce earthquake, respectively. Other symbols and notations are the same as in Fig. 11.

Karadere–Düzce branch of the NAF in the 6 months after the 1999 İzmit earthquake (Fig. 1). A waveform cross-correlation technique (Aster & Scott 1993) is used to identify similar earthquake clusters in a data set of ∼18 000 events. Depending on the applied similarity criterion, approximately 4–60 per cent of the events belong to similar earthquake clusters (Figs 2–7; Table 1). The average splitting parameters generated by the events in each cluster indicate that the crustal anisotropy varies significantly over small changes in the earthquake and station locations (Figs 9 and 10). This result is compatible with our previous conclusion on a shallow anisotropy in this area (Peng & Ben-Zion 2004). Apparent change of average delay times of up to 30 per cent are observed at stations near the epicentral region of the Düzce main shock (Figs 11 and 12). However, we also find strong changes in the seismicity pattern following the Düzce main shock (Figs 8 and 11a). The large spatial variations of anisotropy can be mapped into apparent temporal changes through the changing seismicity. The analysis of splitting parameters measured within repeating earthquake clusters supports this interpretation, and puts an upper bound of ∼2 per cent change in the delay time associated with the Düzce main shock (Figs 13–15).

Repeating event clusters with similarity criterion $\beta_c = 0.95$ are used in a high-resolution examination of temporal changes of crustal anisotropy. Such a choice would reject earthquake pairs that could potentially produce large temporal variations of anisotropy parameters, resulting in a possible bias toward lower values of temporal changes. However, the mere existence of highly similar waveforms with $\beta_c = 0.95$ near the hypocentral region of the Düzce main shock indicates that the temporal variations of splitting parameters cannot be large (e.g. Bokelmann & Harjes 2000; Liu *et al.* 2004, 2005). On the other hand, the splitting parameters vary significantly for slight changes of propagation paths, indicating that the generating anisotropic structure is spatially heterogeneous and shallow. Mixing temporal with spatial variations of crustal anisotropy can be the main source of uncertainty in observational works and may result in artificially large apparent temporal changes. The use of repeating clusters with high similarity criteria can remove the dependence of the splitting parameters on spatial variations, and allow high-resolution examination of temporal changes within each cluster.

There is a long history of efforts to use temporal changes of observed crustal properties for earthquake forecasting (e.g. Scholz *et al.* 1973). Analysis of shear wave splitting was proposed as an effective tool for obtaining such information (e.g. Gupta 1973; Crampin *et al.* 1990, 1991, 1999, 2004; Crampin & Gao 2005; Teanby *et al.* 2004). However, these claims have been controversial (e.g. Ryall & Savage 1974; Aster *et al.* 1990, 1991; Savage

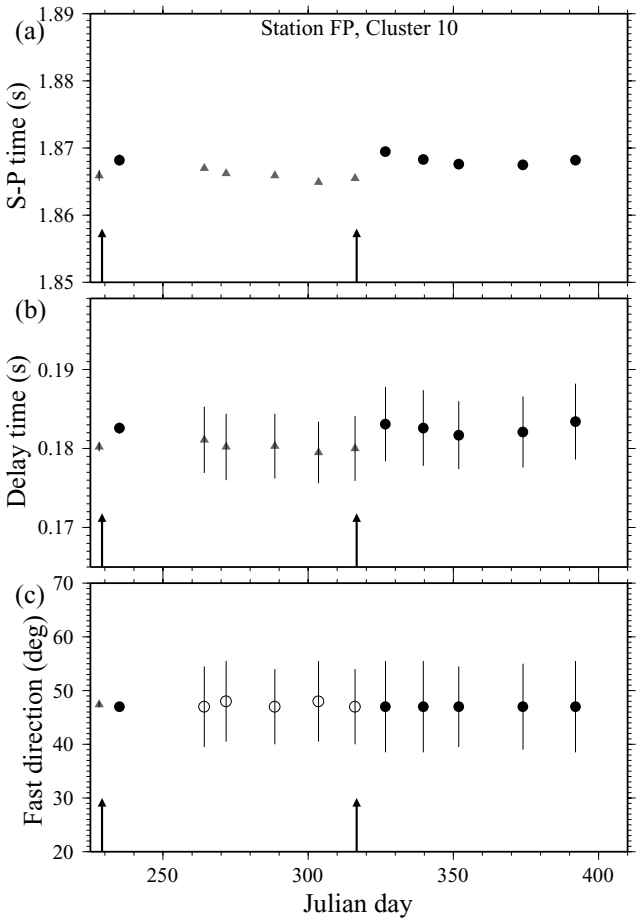

Figure 13. Splitting measurements for the 10 events in cluster C10 with similarity criterion $\beta_c = 0.95$ at station FP. The centroid location of this cluster is shown in Fig. 6. (a) The *S–P* times obtained from the waveform cross-correlation alignment with that of the first event. The average *S–P* times before and after the Düzce earthquakes are marked on the left. The two arrows mark the occurrence time of the İzmit and Düzce earthquakes. (b) Delay times plotted against the event occurrence times for the 10 earthquakes. The vertical line denotes the standard deviations of each measurement. Other symbols are the same as in (a). (c) Fast directions plotted against the event occurrence times. Other symbols are the same as in (a).

et al. 1990; Munson *et al.* 1995; Seher & Main 2004). Liu *et al.* (2004, 2005) examined shear wave splitting in the aftershock region of the 1999 Chi-Chi earthquake using high-quality borehole seismic records. The results did not show a systematic evolution of splitting parameters that may provide reliable precursory information. Similarly, the high-resolution results of the present work do not show (Figs 14 and 15) systematic evolution of splitting parameters either before or after the Duzce main shock. The highly anisotropic, mechanically passive, shallow portion of the crust (e.g., the top 1–3 km) is likely to mask temporal variations of material properties near earthquake nucleation zones in the seismogenic portion of the crust. This may explain the observed lack of reliable precursory evolution of crustal anisotropy in this work, that of Liu *et al.* (2004, 2005) and other studies.

ACKNOWLEDGMENTS

We are grateful to John Armbruster, David Okaya, Naside Ozer and Nano Seeber for essential help with the field work, and to PASSCAL for providing the equipment and technical support for the experiment. We thank Rick Aster, Götz Bokelmann, Elizabeth Cochran, Yunfeng Liu and Paul Silver for useful discussions. The manuscript benefited from valuable comments by the editor Torsten Dahm and referees Nick Teanby and Vaclav Vavryčuk. Fig. 8 was generated using the ZMAP software package (Wiemer 2001). The other figures were generated using GMT (Wessel & Smith 1998). The study was supported by the National Science Foundation (grant EAR0003401).

REFERENCES

Aster, R.C. & Scott, J., 1993. Comprehensive characterization of waveform similarity in microearthquake data sets, *Bull. seism. Soc. Am.,* **83,** 1307–1314.

Aster, R.C., Shearer, P.M. & Berger, J., 1990. Quantitative measurements of shear wave polarizations at the Anza seismic network, southern California: implications for shear wave splitting and earthquake prediction, *J. geophys. Res.,* **95,** 12 449–12 473.

Aster, R.C., Shearer, P.M. & Berger, J., 1991. Comments on 'Quantitative measurements of shear-wave polarization at the Anza seismic network, Southern California: implications for shear-wave splitting and earthquake prediction' by Aster, R.C., Shearer, P.M. & Berger J.—Reply, *J. geophys. Res.,* **96,** 6415–6419.

Ben-Zion, Y. & Sammis, C.G., 2003. Characterization of fault zones, *Pure appl. Geophys.,* **160,** 677–715.

Ben-Zion, Y. *et al.,* 2003. A shallow fault zone structure illuminated by trapped waves in the Karadere-Düzce branch of the North Anatolian Fault, western Turkey, *Geophys. J. Int.,* **152,** 699–717.

Bokelmann, G.H.R. & Harjes, H.P., 2000. Evidence for temporal variation of seismic velocity within the upper continental crust, *J. geophys. Res.,* **105,** 23 879–23 894.

Cochran, E.S., Vidale, J.E. & Li, Y.-G., 2003. Near-fault anisotropy following the Hector Mine earthquake, *J. geophys. Res.,* **108**(B9), 2436, doi:10.1029/2002JB002352.

Crampin, S. & Chastin, S., 2003. A review of shear wave splitting in the crack-critical crust, *Geophys. J. Int.,* **155,** 221–240.

Crampin, S. & Gao, Y., 2005. Comment on 'Systematic analysis of shear-wave splitting in the aftershock zone of the 1999 Chi-Chi, Taiwan, earthquake: shallow crustal anisotropy and lack of precursory variations' by Liu, Y., Teng, T.-L. & Ben-Zion, Y., *Bull. seism. Soc. Am.,* **95,** 354–360, doi:10.1785/0120040092.

Crampin, S., Booth, D.C., Evans, R., Peacock, S. & Fletcher, J.B., 1990. Change in shear wave splitting at Anza near the time of the North Palm Springs earthquake, *J. geophys. Res.,* **95,** 11 197–11 212.

Crampin, S., Booth, D.C., Evans, R., Peacock, S. & Fletcher, J.B., 1991. Comment on 'Quantitative measurements of shear wave polarizations at the Anza seismic network, Southern California: Implications for shear wave splitting and earthquake predication' by Aster, R.C., Shearer, P.M. & Berger, J., *J. geophys. Res.,* **96,** 6403–6414.

Crampin, S., Volti, T. & Stefánsson, R., 1999. A successfully stress-forecast earthquake, *Geophys. J. Int.,* **138,** F1–F5.

Crampin, S., Volti, T. & Stefánsson, R., 2004. Response to 'A statistical evaluation of a "stress-forecast" earthquake' by T. Seher & I.G. Main, *Geophys. J. Int.,* doi: 10.1111/j.1365-246X.2004.02187.x.

Davis, J.C., 1986. *Statistics and Data Analysis in Geology,* John Wiley, Hoboken, NJ.

Gao, Y., Wang, P., Zheng, S., Wang, M. & Chen, Y.-T., 1998. Temporal changes in shear-wave splitting at an isolated swarm of small earthquakes in 1992 near Dongfang, Hainan Island, Southern China, *Geophys. J. Int.,* **135,** 102–112.

Gupta, I.N., 1973. Premonitory variations in *S*-wave velocity anisotropy before earthquakes in Nevada, *Science,* **182,** 1129–1132.

Habermann, R.E., 1983. Teleseismic detection in the Aleutian Island Arc, *J. geophys. Res.,* **88,** 5056–5064.

Igarashi, T., Matsuzawa, T. & Hasegawa, A., 2003. Repeating earthquakes and interplate aseismic slip in the northeastern Japan subduction zone, *J. geophys. Res.,* **108**(B5), 2249, doi:10.1029/2002JB001920.

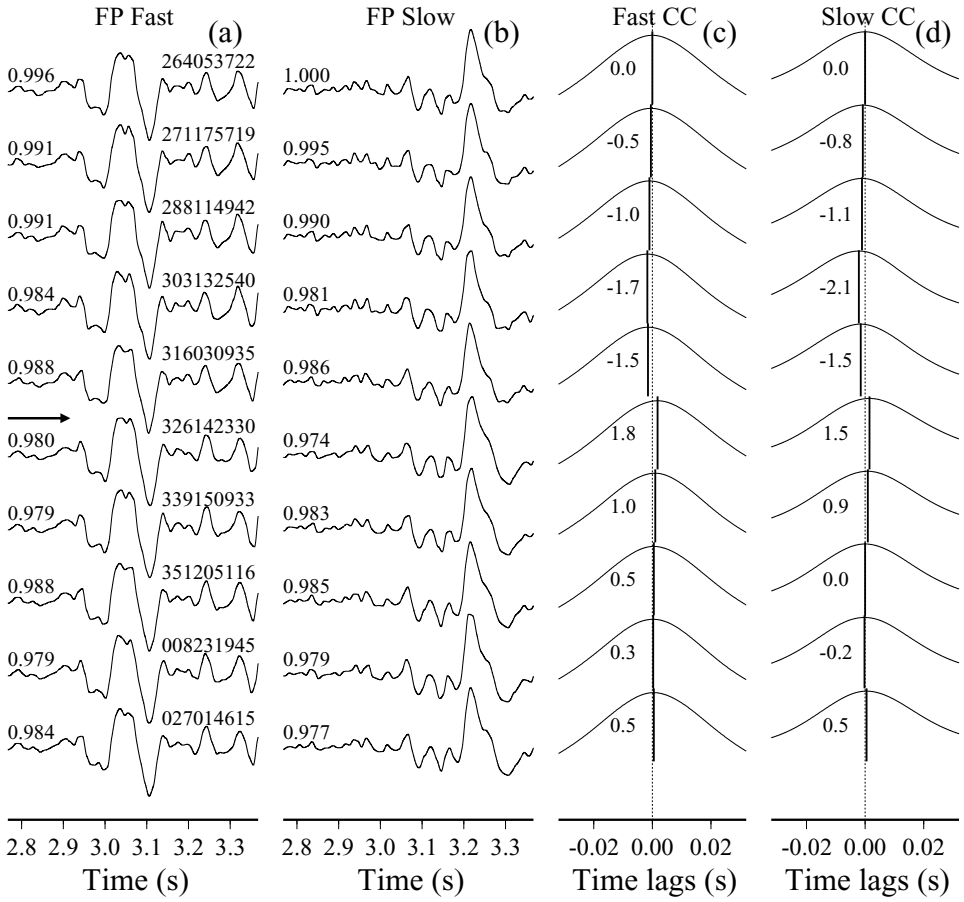

Figure 14. Fast (a) and slow (b) component seismograms for 10 events in cluster C10 at station FP. The seismograms are aligned with *P*-wave arrivals at 1 s and rotated into fast and slow components using an average fast direction of 45.6°. The event ID is shown on right of each seismogram in panel (a). The cross-correlation coefficients relative to the first seismogram are marked on left of each trace. The cross-correlation functions between the first and subsequent fast (c) and slow (d) seismograms. The peak time lags are marked by short thick vertical lines on top of the fast and slow cross-correlation functions. The value of the time lags in ms is also shown on the left of each vertical line.

Klein, F.W., 1978. *Hypocenter Location Program HYPOINVERSE,* Open File Report 78-694, US Geological Survey, Boulder, CO.

Leary, P.C., Crampin, S. & McEvilly, T.V., 1990. Seismic fracture anisotropy in the Earth's crust: an overview, *J. geophys. Res.,* **95**(7), 11 105–11 114.

Lees, J.M., 1998. Multiplet analysis at Coso Geothermal, *Bull. seism. Soc. Am.,* **88**(5), 1127–1143.

Liu, Y., Teng, T.-L. & Ben-Zion, Y., 2005. Systematic analysis of shear-wave splitting in the aftershock zone of the 1999 Chi-Chi earthquake: shallow crustal anisotropy and lack of precursory variations, *Bull. seism. Soc. Am.,* **94,** 2330–2347.

Liu, Y., Teng, T.-L. & Ben-Zion, Y., 2005. Reply to Comment of Crampin and Gao on 'Systematic analysis of shear-wave splitting in the aftershock zone of the 1999 Chi-Chi, Taiwan, earthquake: shallow crustal anisotropy and lack of precursory variations', *Bull. seism. Soc. Am.,* **95,** 361–366, doi:10.1785/0120040109.

Lyakhovsky, V., Ben-Zion, Y. & Agnon, A., 2001. Earthquake cycle, fault zones and seismicity patterns in a rheologically layered lithosphere, *J. geophys. Res.,* **106,** 4103–4120.

Mardia, K.V. & Jupp, P.E., 2000. *Directional Statistics,* John Wiley, Hoboken, NJ.

Munson, C.G., Thurber, C.H., Li, Y. & Okubo, P.G., 1995. Crustal shear wave anisotropy in southern Hawaii: spatial and temporal analysis, *J. geophys. Res.,* **100**(B10), 20 367–20 377.

Nadeau, R.M., Antolik, M., Johnson, P.A., Foxall, W. & McEvilly, T.V., 1994. Seismological studies at Parkfield III: microearthquake clusters in the study of fault-zone dynamics, *Bull. seism. Soc. Am.,* **84,** 247–263.

Nadeau, R.M., Foxall, W. & McEvilly, T.V., 1995. Clustering and periodic recurrence of microearthquakes on the San Andreas Fault at Parkfield, California, *Science,* **267,** 503–507.

Niu, F., Silver, P.G., Nadeau, R.M., McEvilly, T.V., 2003. Stress-induced migration of seismic scatterers associated with the 1993 Parkfield aseismic transient event, *Nature,* **426,** 544–548.

Peng, Z. & Ben-Zion, Y., 2004. Systematic analysis of crustal anisotropy along the Karadere-Düzce branch of the north Anatolian fault, *Geophys. J. Int.,* **159,** 253–274.

Poupinet, G., Ellsworth, W.L. & Frechet, J., 1984. Monitoring velocity variations in the crust using earthquake doublets: an application to the Calaveras Fault, California, *J. geophys. Res.,* **89,** 5719–5731.

Press, W., Flannery, B., Teukolsky, S. & Vetterling, W., 1986. *Numerical Recipes,* Cambridge University Press, Cambridge.

Rabbel, W., 1994. Seismic anisotropy at the Continental Deep Drilling Site (Germany), *Tectonophysics,* **232,** 329–341.

Reilinger, R.E. *et al.*, 1997. Global Positioning System measurements of the present day crustal movements in the Arabia-Africa-Eurasia plate collision zone, *J. geophys. Res.,* **102,** 9983–9999.

Rubin, A.M., Gillard, D. & Got, J.-L., 1999. Streaks of microearthquakes along creeping faults, *Nature,* **400,** 635–641.

Ryall, A. & Savage, W., 1974. *S* wave splitting: key to earthquake prediction?, *Bull. seism. Soc. Am.,* **64,** 1943–1951.

Saiga, A., Hiramatsu, Y., Ooida, T. & Yamaoka, K., 2003. Spatial variation in the crustal anisotropy and its temporal variation associated with a moderate-sized earthquake in the Tokai region, central Japan, *Geophys. J. Int.,* **154,** 695–705.

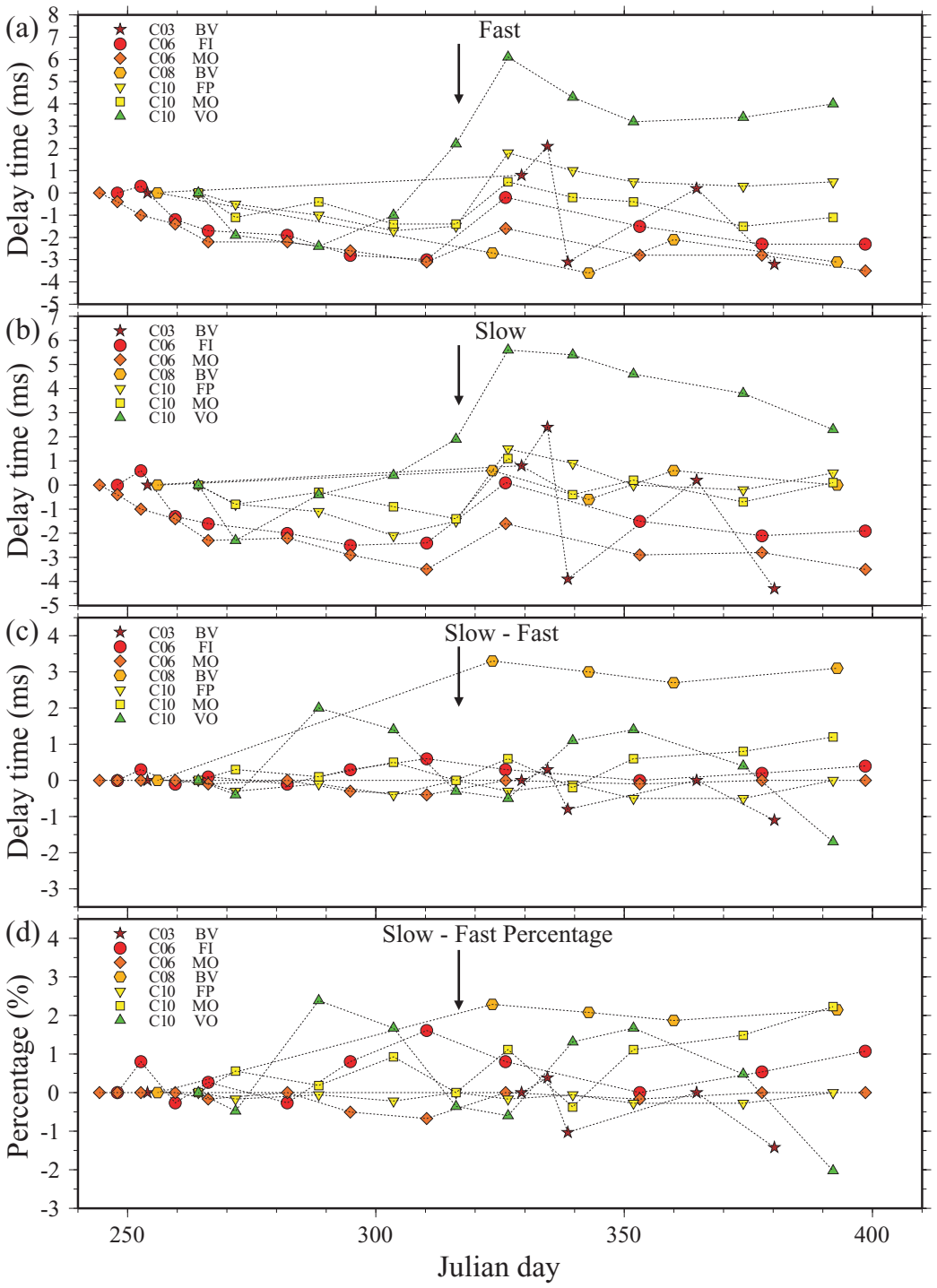

Figure 15. Relative delay times of the fast (a) and slow (b) waves plotted against the earthquake occurrence time for four repeating earthquake clusters with similarity criterion $\beta_c = 0.95$ at five stations. The relative delay times are calculated via waveform cross-correlation as shown in Fig. 14. The vertical line marks the occurrence time of the Düzce main shock. (c) The difference of the relative delay times between the fast and slow waves plotted against the earthquake occurrence time. (d) The changes of delay times between fast and slow shear waves as a percentage plotted against the earthquake occurrence time. The percentage is calculated by dividing the relative delay times in (c) with the average values of the delay times between fast and slow shear waves obtained by Peng & Ben-Zion (2004).

Savage, M.K., Peppin, W.A. & Vetter, U.R., 1990. Shear wave anisotropy and stress direction in and near Long Valley caldera, California, 1979–1988, *J. geophys. Res.,* **95,** 11 165–11 177.

Schaff, D.P., Bokelmann, G.H.R., Beroza, G.C., Waldhauser, F. & Ellsworth, W.L., 2002. High-resolution image of Calaveras Fault seismicity, *J. geophys. Res.,* **107**(B9), 2186, doi:10.1029/2001JB000633.

Scholz, C.H., 2002. *The Mechanics of Earthquakes and Faulting,* Cambridge University Press, New York.

Scholz, C.H., Sykes, L.R. & Aggarwal, Y.P., 1973. Earthquake prediction: a physical basis, *Science,* **181,** 803–810.

Seeber, L., Armbruster, J.G., Ozer, N., Aktar, M., Baris, S., Okaya, D., Ben-Zion, Y. & Field, E., 2000. The 1999 Earthquake sequence along the

North Anatolia Transform at the juncture between the two main ruptures, in *The 1999 İzmit and Düzce Earthquakes: Preliminary Results,* pp. 209–223, eds. Barka, A., Kozaci, O., Akyuz, S., Altunel, E., Istanbul Technical University, Istanbul.

Seher, T. & Main, I.G., 2004. A statistical evaluation of a 'stress-forecast' earthquake, *Geophys. J. Int.,* **157**(1), 187–193, doi:10.1111/j.1365-246X.2004.02186.x.

Shearer, P.M., Hardebeck, J.L., Astiz, L. & Richards-Dinger, K.B., 2003. Analysis of similar event clusters in aftershocks of the 1994 Northridge, California, earthquake, *J. geophys. Res.,* **108**(B1), 2035, doi:10.1029/2001JB000685.

Tadokoro, K. & Ando, M., 2002. Evidence for rapid fault healing derived from temporal changes in S wave splitting, *Geophys. Res. Lett.,* **29**(4), 1047, doi:10.1029/2001GL013644.

Tadokoro, K., Ando, M. & Umeda, Y., 1999. S wave splitting in the aftershock region of the 1995 Hyogo-ken Nanbu earthquake, *J. geophys. Res.,* **104,** 981–991.

Teanby, N., Kendall, J.-M., Jones, R.H. & Barkved, O., 2004. Stress-induced temporal variations in seismic anisotropy observed in microseismic data, *Geophys. J. Int.,* **156**(3), 459–466, doi:10.1111/j.1365-246X.2004.02212.x.

Utkucu, M., Nalbant, S.S., McCloskey, J., Steacy, S. & Alptekin, O., 2003. Slip distribution and stress changes associated with the 1999 November 12, Düzce (Turkey) earthquake (Mw = 7.1), *Geophys. J. Int.,* **153,** 229–241.

Vavryčuk, V., 1993. Crustal anisotropy from local observations of shear-wave splitting in West Bohemia, Czech Republic, *Bull. seism. Soc. Am.,* **83,** 1420–1441.

Wessel, P. & Smith, W.H.F., 1998. New, improved version of the Generic Mapping Tools released, *EOS, Trans. Am. geophys. Un.,* **79,** 579.

Wiemer, S., 2001. A software package to analyse seismicity: ZMAP, *Seism. Res. Lett.,* **72,** 373–382.

Zhang, Z. & Schwartz, S.Y., 1994. Seismic anisotropy in the shallow crust of the Loma Prieta segment of the San Andreas fault system, *J. geophys. Res.,* **99**(B5), 9651–9661.